Vortex dislocation in the near wake of a cylinder with span-wise variations in diameter

Fatma Ayancik[1], Lars Siegel[2], Guosheng He[1,3], Arne Henning[2], Karen Mulleners[1,*]

1: Institute of Mechanical Engineering, École polytechnique fédérale de Lausanne (EPFL), Switzerland
2: German Aerospace Center (DLR), Inst. for Aerodyn. & Flow Tech., Göttingen, Germany
3: Beijing University of Technology, China
*Corresponding author: karen.mulleners@epfl.ch

Keywords: vortex dislocation, intermittency, oblique shedding

ABSTRACT

We examined the evolution of three-dimensional vortex shedding patterns induced by spanwise variations of the cylinder diameter. Two distinct types of shedding patterns have identified through flow visualization: continuous (in-phase) oblique shedding where vortices shed with lower frequency stay attached to the vortices with higher frequency without any discontinuity or splitting and discontinuous (out-of-phase) shedding where the lower frequency vortices have no attachment to higher frequency vortices and vortex dislocation occurs. The dislocation seen in the flow is strongly influenced by the spanwise irregularities. We observed a clear and strong in-phase spanwise vortex shedding for the three smooth cylinder configurations tested in the study. The tapered, bumps and steps configurations showed sections of strong coherent spanwise vortex shedding, and we identified hardly any coherent structures for the rib, sinusoidal, and helical configurations. Depending on the geometry and number of spanwise irregularities, incoherent structures make difficult to determine the occurrence and location of vortex dislocations in the cylinder wake without a method that enables a reduction in the complexity. Here, we introduce a numerical approach that obtains the dominant structures of vortex shedding patterns by reducing the complexity in noisy data. The method maps the variations in the oblique shedding angle over time and provide quantitative conclusions on the intermittent occurrence and location of vortex dislocations in the $15\,000$ snapshots taken for each of the different cylinder geometries regardless of turbulence.

1. Introduction

Cylindrical structures are encountered in numerous engineering designs for support and attachment. The towers of wind and tidal turbine, the hull of a spar platform and deep-water risers are a few examples of these designs. The periodic shedding of vortices around those structures induces vibrations that lead to amplified fatigue damage, increased drag forces and aeroacoustic noise generation. To suppress vortex induced vibrations and reduce the magnitude of fluctuating lift and mean drag forces, cylindrical supporting structures are equipped with a surface protrusions such as helical strakes or wires, and hemispherical bumbs in a spiral pattern (M. Zdravkovich,

1981; Owen et al., 2001; Lam et al., 2004). The discontinuities introduced by surface protrusions perturb the two dimensional periodic vortex shedding in the wake of the cylinder. They lead to the formation of span-wise cells where vortices are shed with a different frequency or a phase shift with respect to the neighboring cells (Williamson, 1992; Dunn & Tavoularis, 2006) creating oblique shedding with a some angle to the cylinder axis. At the interface between different cells, vortices break the continuity of the main vortex core and dislocate. The phenomenon of vortex dislocation has been studied experimentally and numerically for cylinders with a stepwise change in diameter (Dunn & Tavoularis, 2006; McClure et al., 2015; Morton & Yarusevych, 2020; Tian et al., 2020). Two distinct types of vortex connection at cell boundaries can be identified: some with lower frequency connecting with higher frequency counterparts and some with half-loop vortex connections. Other studies focused on the three dimensional wake patterns and vortex dislocation behind sinusoidal wavy cylinders (Lam et al., 2004; Bai et al., 2019; Liu et al., 2019) and confirmed that the vortex streets differ from the structures seen on circular cylinders. For circular cylinders, wake are more regular. The wake of the wavy cylinders shows incoherent shedding due to span wise effects. For a large range of Reynolds numbers, even in the wake of a smooth cylinder with a uniform diameter, three dimensional vortex patterns emerge naturally (M. M. Zdravkovich, 1996; Braza et al., 2001). The interaction between the vortices in the different shedding cells lead to frequency modulations in the wake (Lewis & Gharib, 1992).

The goal of past research was to examine vortex interactions and dislocations in idealized cylinder configurations to understand more complex patterns in bluff-body wakes and generate non-uniform vortex shedding in a controlled manner. Yet, there has been no automated attempt to determine the vortex dislocations. Here, we summarize the main points of the vortex dislocation phenomenon for cylinders with span-wise variations in diameter. Then, we provide an approach which determines the oblique shedding angle and intermittent occurrence of vortex dislocations in the cylinder wake.

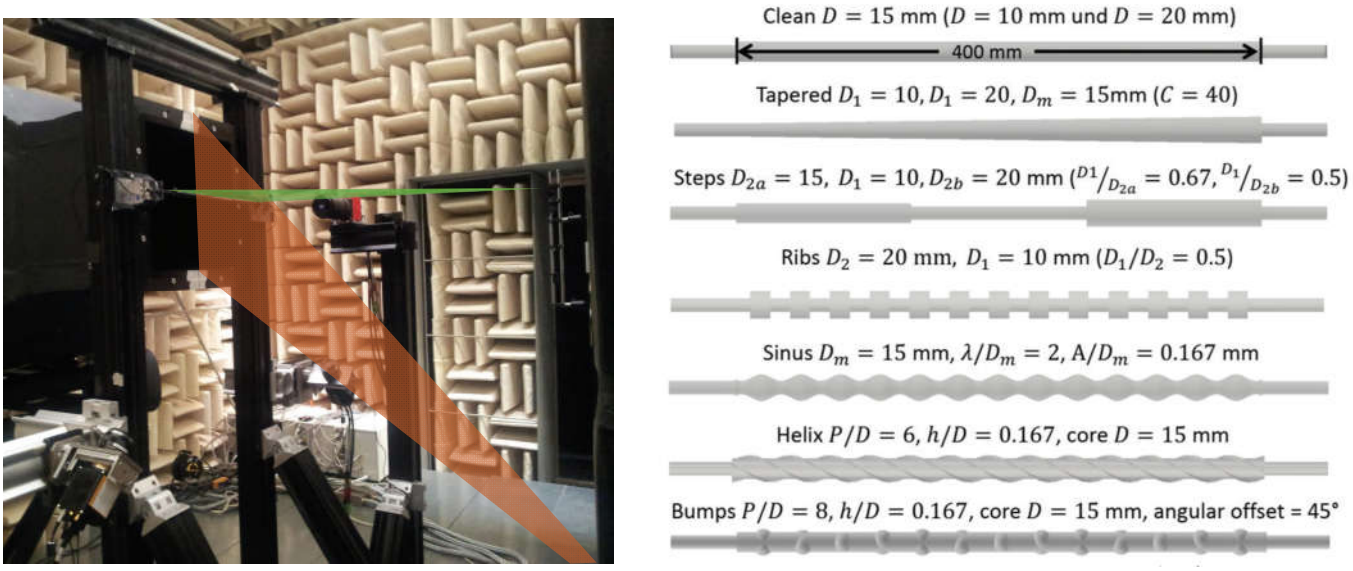

Figure 1. Experimental setup with indicated light sheets for the 2C2D-PIV (orange) and 3C2D-PIV (green) (left); and the different cylinders tested (right).

We believe that this is the initial step to automatize the determination process.

2. Methodology

2.1. Experimental methods

Synchronous particle image velocimetry (PIV), force and microphone measurements are performed in a circular wind tunnel with a nozzle size of $0.4\,\mathrm{m} \times 0.4\,\mathrm{m}$ at a maximum flow speed of $\mathrm{U}_\infty = 43\,\mathrm{m/s}$. The test section is surrounded by a full anechoic chamber of approximately $9\,\mathrm{m} \times 9\,\mathrm{m} \times 5\,\mathrm{m}$. All three velocity components (3C) are acquired using stereoscopic or 3C2D-PIV in a horizontal span- and flow-wise oriented plane in the near wake of the cylinder. A total number of $15\,000$ statistically independent PIV snapshots have been recorded with an acquisition rate of $10\,\mathrm{Hz}$. The pressure measurements are conducted simultaneously with 4 microphones (Type:1/4 40BF; G.R.A.S.) in the far field outside the flow to avoid unwanted influences on the flow field and vice versa. The microphones are installed above the cylinder and are distributed in a horizontal line at the mid-span of the cylinders in flow direction to take into account the directivity of the sound emission. The vertical positions were approximately $1.8\,\mathrm{m}$ ($120\,d$) above the cylinder and the distance between the microphones was about $0.3\,\mathrm{m}$ ($20\,d$). A multi-analyzer (Type: DEWE3; Dewetron) simultaneously records the microphone-signals, the camera trigger, the q-switch of the laser and three components of the forces acting on the cylinders with a sampling frequency of $f_s = 100\,\mathrm{kHz}$ and a dynamic range of $24\,\mathrm{bit}$.

A set of six cylinders with different span-wise variations are investigated as illustrated in fig. 1. The geometric parameters of the cylinders are selected such that the core or the average diameter $\overline{D}$ is $15\,\mathrm{mm}$ and the span-wise wavelength for the repeated variations are constant. The Reynolds number based in the average cylinder diameter is $43\,000$. In addition, three smooth cylinders with a uniform diameter of $10\,\mathrm{mm}$, $15\,\mathrm{mm}$, and $20\,\mathrm{mm}$ have been measured.

2.2. Proper orthogonal decomposition

The proper orthogonal decomposition (POD) method gives an orthogonal basis to approximate a given set of data in a least square sense based on the energy content (Lumley, 1970). The general idea behind POD is to decompose the flow field, $\mathbf{u}(x, y, t_n)$, into a set of deterministic spatial eigenmodes $\boldsymbol{\psi_i}(x, y)$ tuned by time-dependent mode coefficients $a_i(t_n)$. POD provides ways to find optimal model reduction approximations for the given flow field.

In the current work, POD was implemented on the two-dimensional, three-component velocity field $\mathbf{u} = (u, v, w)$ obtained by means of PIV based on the snapshot method as,

$$\mathbf{u}(x, y, t_n) = \sum_{i=1}^{N} a_i(t_n)\boldsymbol{\psi_i}(x, y) \tag{1}$$

where N is the number of time instantaneous field realizations.

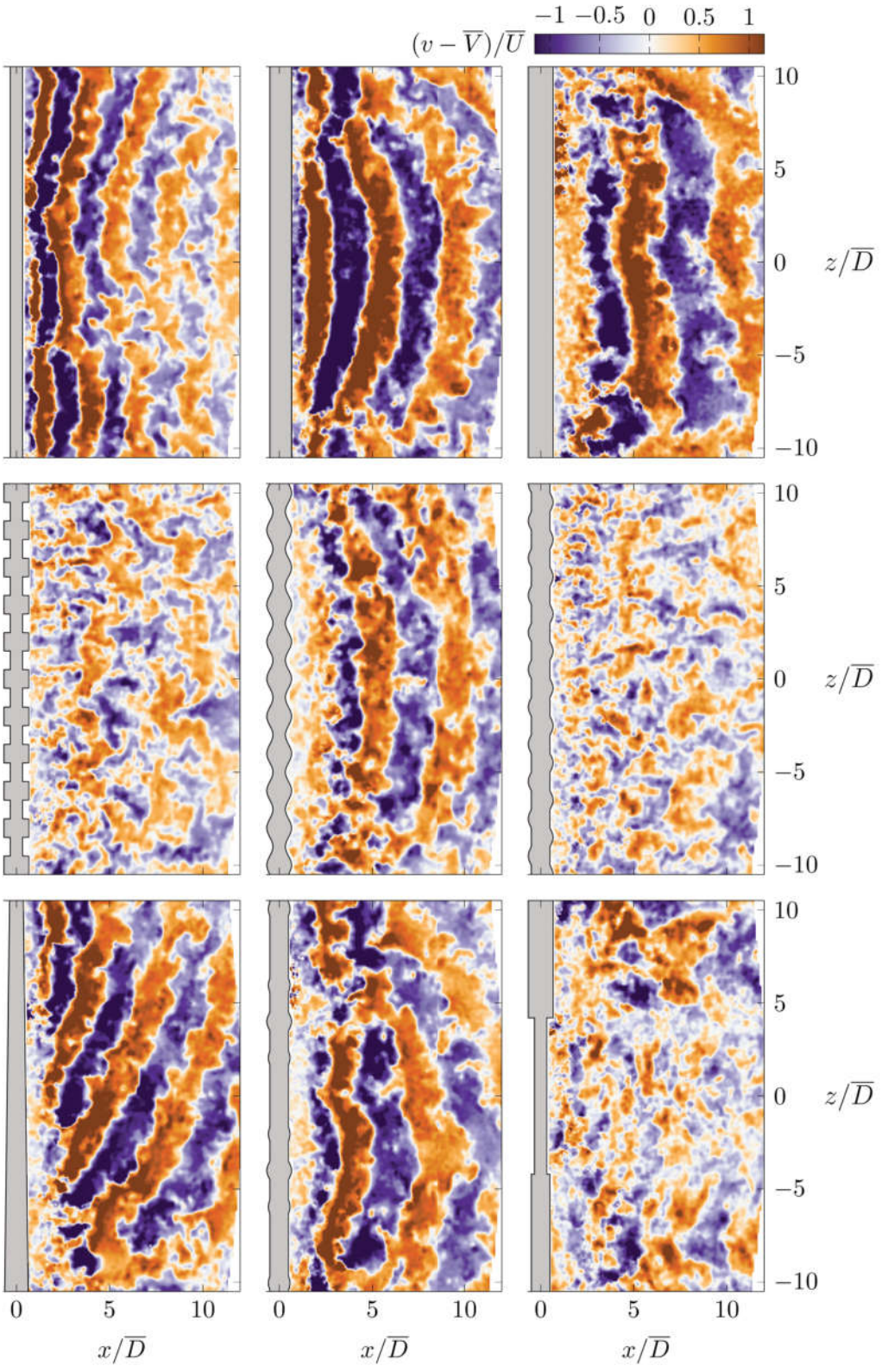

Figure 2. Instantaneous snapshots of the out-of-plane velocity fluctuations in the horizontal plane in the wake of all cylinders: (top) clean cylinders; (middle) rib, sinusoidal, helical; (bottom) tapered, bumbs, steps.

3. Results and discussion

3.1. Wake analysis

Figure 2 shows a snapshot of the instantaneous fluctuations of the out-of-plane velocity component in the horizontal plane in the wake of all cylinders tested in the study. The axis are scaled with the average cylinder diameter $\overline{D}$ and $\overline{W}$ is the average out-of-plane velocity component. For the three smooth cylinder configurations, a clear and strong span wise vortex shedding can be observed. With increasing diameter, the flow structures of the same velocity orientation become wider, which is consistent with the decreasing vortex shedding frequency. For the rib, sinusoidal, and helical configurations, vortex interactions occur more frequently than clean cylinders and almost no coherent structures appear. All velocity fields are characterized by many turbulent fluctuations. In addition, the amplitude of out-of-plane velocity component is lower. This effect is strongest in the helix configuration, in the case of the sinusoidal cylinder, we can still observe traces of coherent structures. The velocity fields of the tapered, bumbs and step configurations have sections of strong span wise vortex shedding. For example, the tapered structure provides oblique but still coherent shedding. In the case of the step cylinder, strong span wise vortex interactions occur at the sharp edges, so that a clear separation of the individual segments can be observed. In the case of the bumpy cylinder, the variously oriented irregularities provide a deformation of the spanwise vortex dislocations. The dislocation of the flow is strongly influenced by the spanwise irregularities.

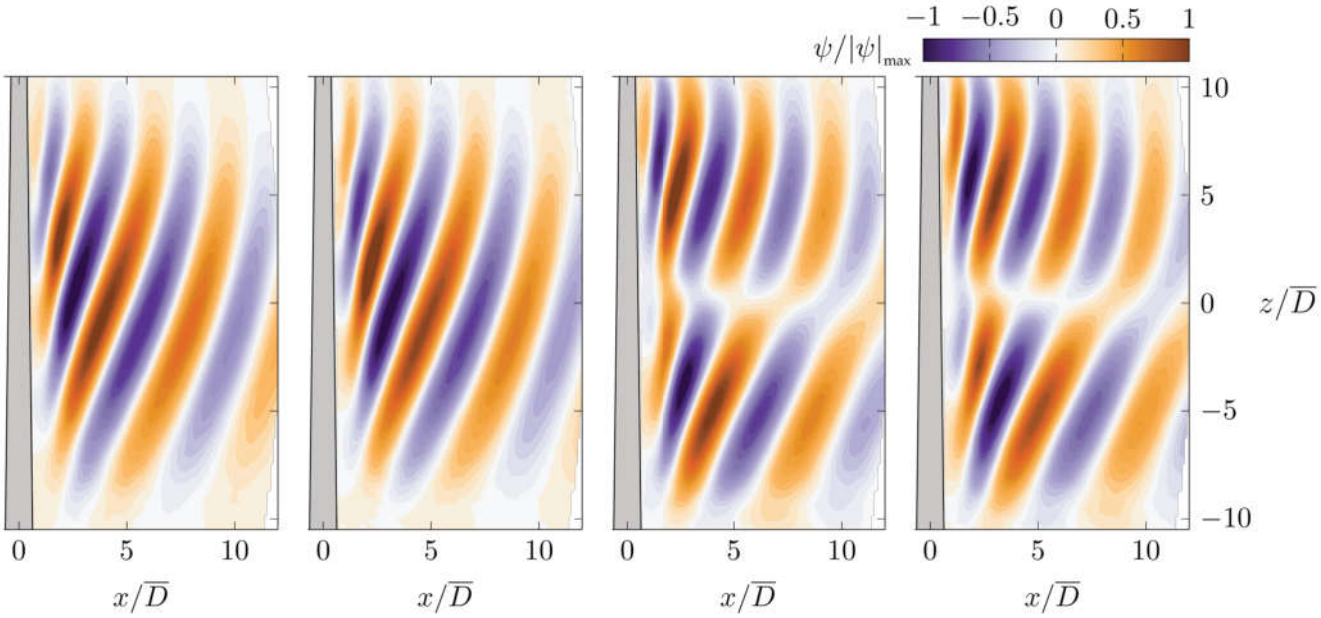

Figure 3. Dominant POD modes of the out-of-plane velocity fluctuations in the horizontal plane in the wake of the tapered cylinder.

POD was performed on the flow field to analyze the dominant vortex shedding pattern in the wake. The first four dominant modes are presented in fig. 3. They form two mode pairs. The first mode pair represent the oblique vortex shedding due to the different natural shedding frequencies behind the different diameters. The second mode pair represents the vortex dislocation occurrence around mid-span. Higher order modes display additional dislocation positions.

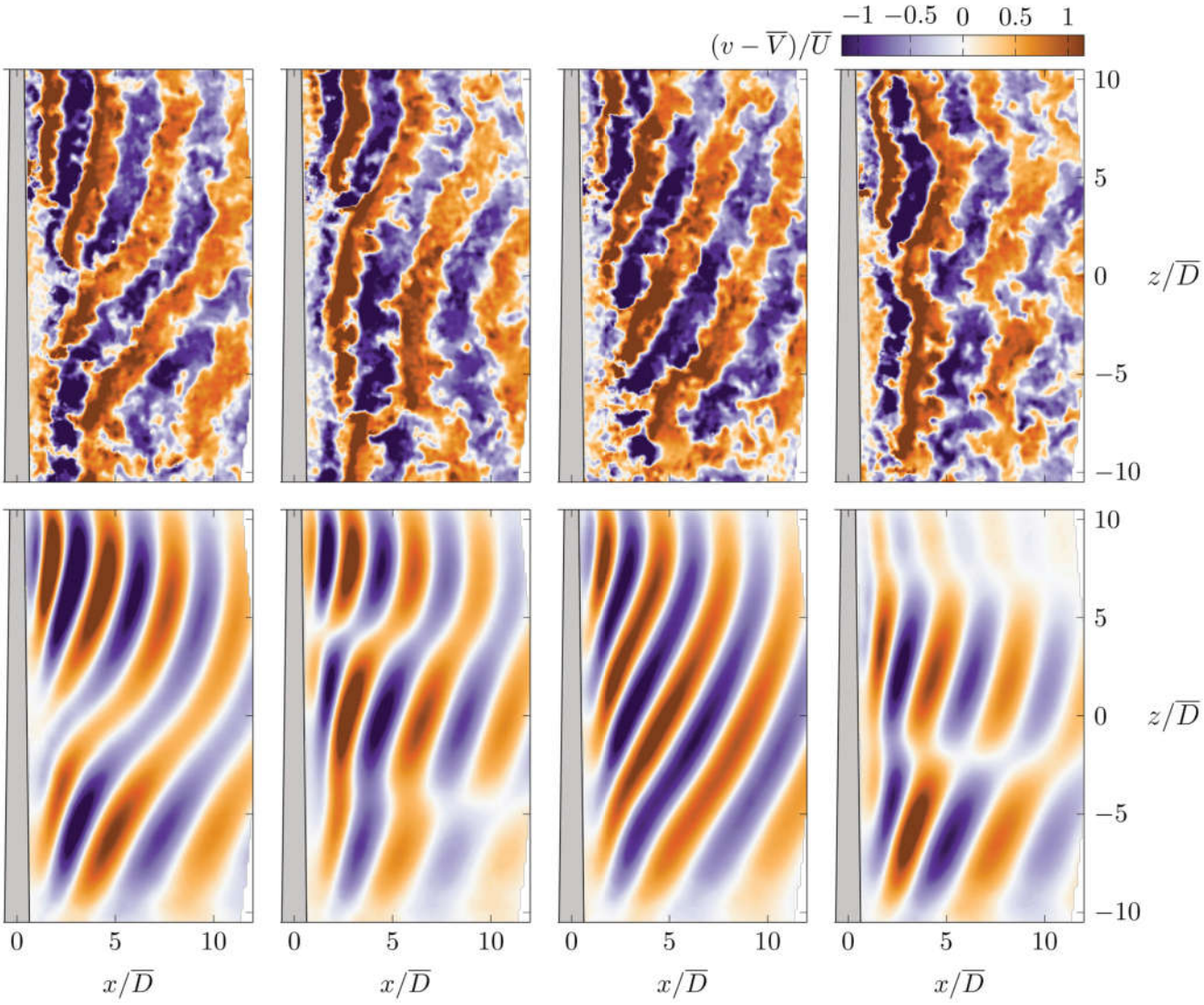

Figure 4. Instantaneous snapshots of the out-of-plane velocity fluctuations in the horizontal plane in the wake of a tapered cylinder (top). Reconstruction of the snapshots based on the first six POD modes (bottom).

Figure 4 (top row) shows four snapshots of the instantaneous fluctuations of the out-of-plane velocity component in the horizontal plane in the wake of the tapered cylinder. Strong oblique coherent structures traveling downstream can be seen in the wake of the tapered cylinder. The vortex shedding behind the smaller diameter end of the cylinder is faster than behind the larger diameter end reflecting the different vortex shedding frequencies along the span. Two out-of-phase wake structures gradually curves along the span from each end of the cylinder and take on the

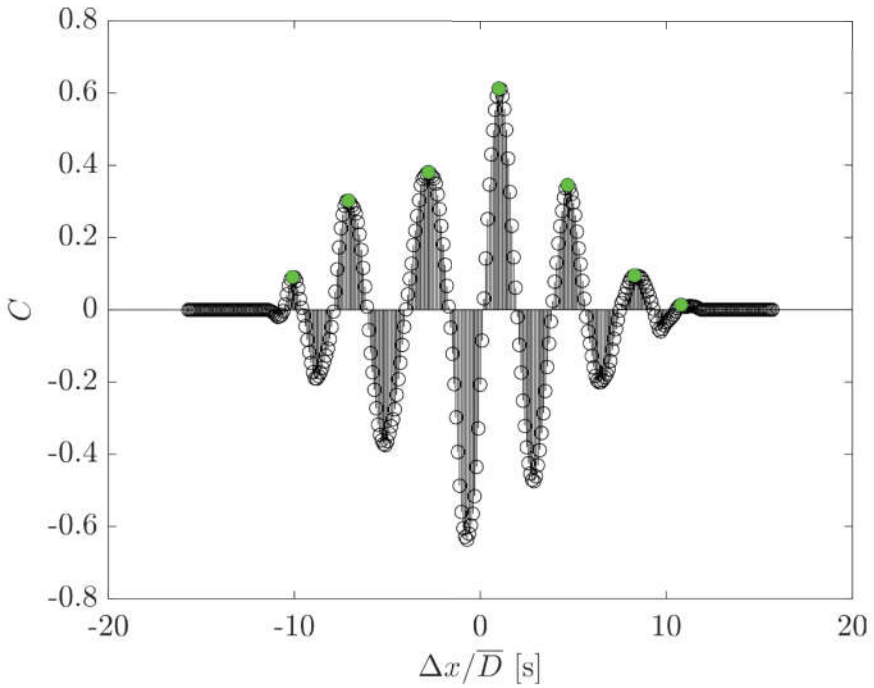

Figure 5. Cross-correlation peaks and their corresponding lags between $z/\overline{D} = 0$ and $z/\overline{D} = 1$ for a clean cylinder

appearance of a semi-chevron like pattern (Williamson, 1992) with two different oblique angles θ. This leads to an oblique detachment of the flow due to the conical shape of the cylinder. The oblique vortex rolls in the wake and occasional break-up and reconnection of successive rolls occur.

3.2. Vortex dislocation identification schemes

The reconstructed out-of-plane velocity fields based on the first six POD modes are presented in the bottom row of fig. 4. Based on the reconstructed images, it is easier to identify whether vortex dislocation occurs or not. Yet, the location of the dislocation does not seem to be correctly represented in some of the reconstructed images. Therefore, we need to revert to different methods to identify the occurrence and location of vortex dislocations.

As a first step towards building an automated process, we propose to use cross-correlation on instantaneous snapshots to (i) obtain the dominant vortex shedding pattern in the wake that captures the general trend of noisy data, (ii) determine the changes of oblique shedding angle and the vortex dislocation location, and (iii) create a time-map that indicates oblique shedding angle variations and vortex dislocation points for all the snapshots obtained in the study.

Cross-correlation measures the similarity of a signal $X_{\mathrm{n}}(x, y)$ and lagged copies of a signal $Y_{\mathrm{n}}(x, y)$ as a function of the lag, Δx. The output returns the distribution of the delay between two signals with associated cross-correlation function, C values as in fig. 5. The maximum of the cross-correlation function indicates the lag where two signals match exactly.

Oblique structures occur and travel downstream in the wake of cylinders due to a phase difference

or different vortex shedding frequencies along the span. Phase difference or different vortex shedding frequencies creates a delay between structures at different positions of the span where we can observe the lag from the instantaneous snapshots but not quantify it. The cross-correlation approach helps to quantify the lag in snaphots, since a single instantaneous velocity snapshot is formed of consecutive velocity signals over the span of a cylinder.

The new approach performs the cross-correlation in between a reference location signal at $z/\overline{D} = 0$ and the signal at a different spanwise location that varies between $-10 \leq z/\overline{D} \leq 10$. In return, for each point along the span, we obtain a lag and an associated cross-correlation value, C By using the dominant correlation peaks, C, as shown in fig. 5 with green points and the associated lags, we can reproduce the dominant vortex shedding pattern in the wake without the effects of noise. From the lag, which is actually a streamwise distance, and spanwise distance between two signals, we can calculate the oblique shedding angle by obtaining the slope of the line between two points in space.

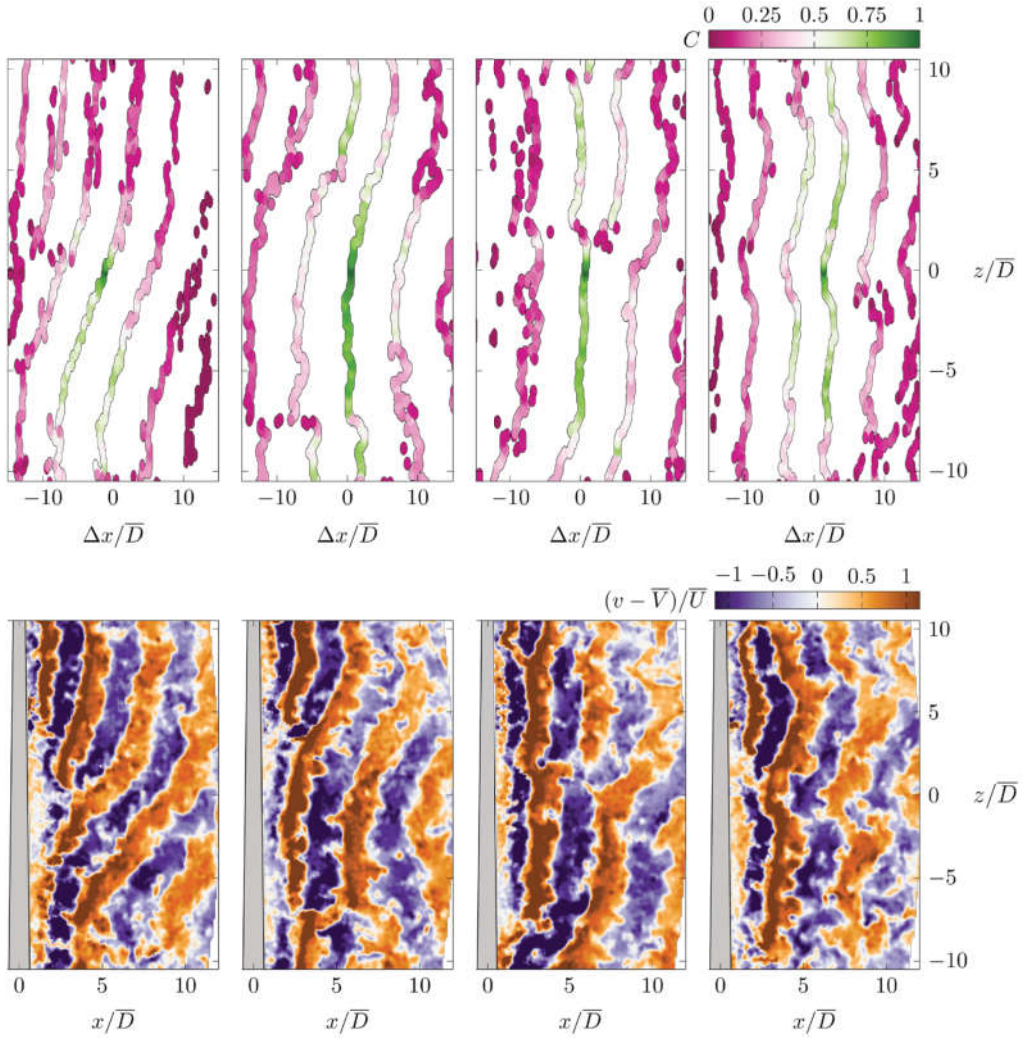

Figure 6. Reproduced of the snapshots based on the dominant peaks of the cross-correlation (top). Instantaneous snapshots of the out-of-plane velocity fluctuations in the horizontal plane in the wake of a tapered cylinder (bottom).

For a tapered cylinder, fig. 6 shows the reproduced images (top) of the instantaneous snaphots (bottom) at different times based on the dominant peaks of the cross-correlation and their corresponding lags. Colorbar indicates the correlation (C) values and markers corresponds to the lags obtained during the full spanwise search. First and the maximum correlation is shown by the midline with the highest correlation value at zero meaning that we perform cross correlation between $z/\overline{D} = 0$ to $z/\overline{D} = 0$. The other lines with negative and positive offset from the midline obtained from the rest of peaks. Different from the reconstructed POD images, the correlation lines clearly capture the location of the dislocations, vortex branching and oblique shedding angle changes seen in the velocity field.

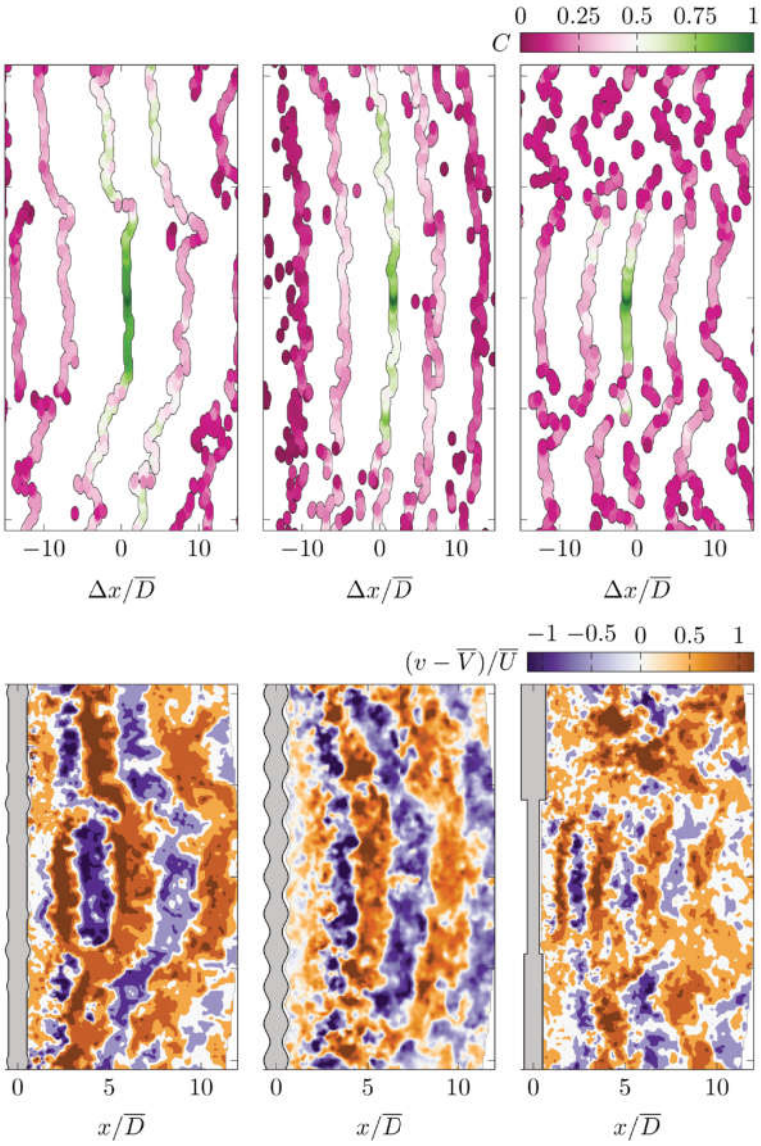

Figure 7. Reproduction of the snapshots based on the dominant peaks of the cross-correlation (top). Instantaneous snapshots of the out-of-plane velocity fluctuations in the horizontal plane in the wake of cylinders hemispherical bumps, sinusoidal waves and steps (bottom).

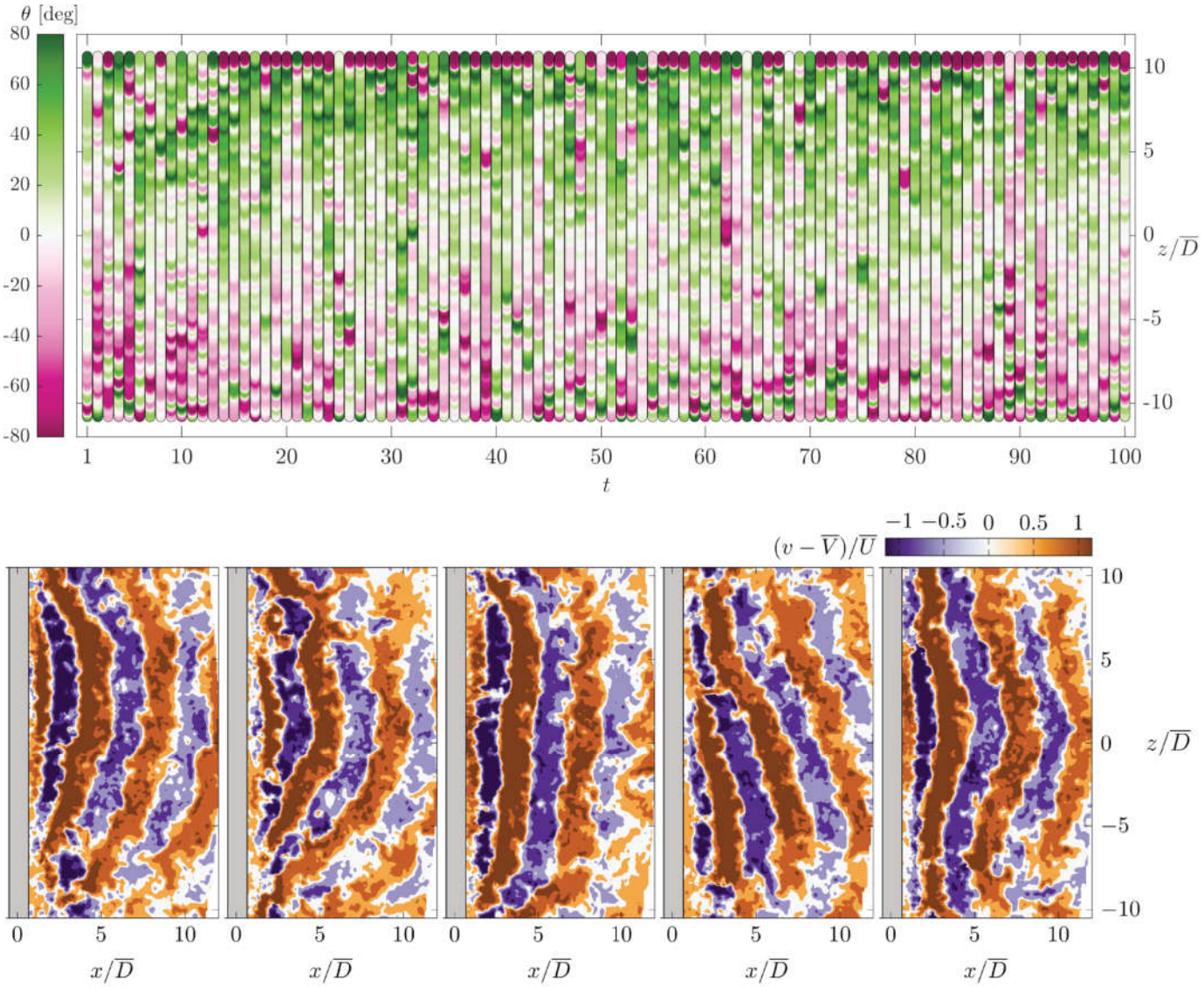

Figure 8. Time map of vortex dislocations and variations in oblique shedding angle seen on clean cylinder wake and selected instantaneous snapshots of the out-of-plane velocity fluctuations at $t = 3$, $t = 5$, $t = 16$, $t = 40$, and $t = 92$.

Figure 7 shows the application of the method on different cylinder shapes. We can capture the vortex shedding patterns even for the cases with strong spanwise vortex interactions and incoherent structures as seen in the cylinder with steps. Around larger diameter area in the step cylinder where the coherent vortex structures are absent but the method still manages to capture the trend.

As a second step, from the slope of the mid correlation line, which corresponds to the maximum correlation peak and its lag at different spanwise locations, we calculated the oblique shedding angle as the angle between vortices to the axis of the cylinder and repeated this process for all the snapshots in the current data. The angle becomes zero when it is perpendicular to the flow direction and it becomes positive or negative in counter clockwise or clockwise direction, respectively. Figure 8 shows the changes in the oblique shedding angle over 100 snapshots for all spanwise locations and some selected instantaneous snapshots for a clean cylinder with a diameter of 15 mm. Colors respresent the oblique shedding angle values along the whole span of a cylinder

varies from $-80° \leq \theta \leq 80°$. When 100 snapshots plotted together, the figure provides a time-map of vortex shedding. Pink markers clustered below the reference line ($z/\overline{D} = 0$) and green markers clustered above the reference line displays the general chevron-like form (Williamson, 1992) vortex shedding as also can be seen in two time snapshots ($t = 3, 92$) of the clean cylinder. Distributed green and pink colored markers with shorter span corresponds to small variations caused by the noise in the data (snapshot at $t = 16$). Every pass around angles close to zero after longer spans correspond to the slope changes indicating the beginning of dislocation. Snapshot at $t = 40$ is one of the example of this trend. The darker colors at close to upper and lower edges of spanwise locations correspond to sudden interruptions or wall effects. The ones close vary between lighter pink or green colors represent the branching in the data (snapshot at $t = 5$). No variation in the angle either pink or green indicates that vortex travels downstream with no variation in the oblique angle meaning that there is no dislocation or indication of dislocation. The new method gives opportunity to reach quantitative conclusions such as x and z locations of the dislocations and oblique shedding angles.

3.3. Outlook

The aim of the study is to characterize the wake topologies behind the different cylinder geometries in detail and to determine the influence of the surface variations on the vortex shedding evolution. More specifically, we are interested in determining the intermittent behavior of the dislocations and quantifying the occurrences and locations. So far, flow visualizations and the new approach helped us to achieve these goals. In future, we plan to extend this method with a data-driven model to automatize the identification and prediction vortex dislocation events. Then, our aim is to link the occurrence of the dislocations to fluctuations in the load and acoustic response.

4. Conclusions

Nine cylinders with different spanwise variations in diameter are investigated to determine the evolution of three-dimensional vortex shedding patterns influenced by spanwise variations. We identified two distinct shedding patterns: continuous oblique shedding without interruption in vortices and discontinuous shedding which leads to dislocation of vortices. For the Reynolds number chosen in the study, we also identified three dimensional vortex patterns in the wake of a smooth cylinder with a uniform diameter confirming (M. M. Zdravkovich, 1996; Braza et al., 2001). Turbulent fluctuations in addition to certain spanwise irregularities hamper the identification of the occurrence and location of vortex dislocations in the cylinder wake. We used a cross-correlation approach that enables a reduction in the complexity and determine the variations in the oblique shedding angle over time and provide quantitative conclusions on the intermittent occurrence and location of vortex dislocations for each of the different cylinder geometries used in the study, and opened up a path for improvement.

Acknowledgements

This work was supported by the Swiss national science foundation Lead Agency programme under grant number 200021E-169841 and the Deutsche Forschungsgemeinschaft (DFG – German Research Foundation) under grant number HE 7369/2-1.

Nomenclature

θ	Oblique shedding angle [deg]
C	Correlation coefficient

References

Bai, H., Alam, M., Gao, N., & Lin, Y. (2019). The near wake of sinusoidal wavy cylinders: Three-dimensional POD analyses. *International Journal of Heat and Fluid Flow*, *75*, 256–277. doi: 10.1016/j.ijheatfluidflow.2019.01.013

Braza, M., Faghani, D., & Persillon, H. (2001). Successive stages and the role of natural vortex dislocations in three-dimensional wake transition. *Journal of Fluid Mechanics*, *439*, 1–41. doi: 10.1017/s002211200100458x

Dunn, W., & Tavoularis, S. (2006). Experimental studies of vortices shed from cylinders with a step-change in diameter. *Journal of Fluid Mechanics*, *555*, 409–437. doi: 10.1017/s002211200600927x

Lam, K., Wang, F., & So, R. (2004). Three-dimensional nature of vortices in the near wake of a wavy cylinder. *Journal of Fluids and Structures*, *19*(6), 815–833. doi: 10.1016/j.jfluidstructs.2004.04.004

Lewis, C. G., & Gharib, M. (1992). An exploration of the wake three dimensionalities caused by a local discontinuity in cylinder diameter. *Physics of Fluids A: Fluid Dynamics*, *4*(1), 104–117. doi: 10.1063/1.858489

Liu, G., Xue, Q., & Zheng, X. (2019). Phase-difference on seal whisker surface induces hairpin vortices in the wake to suppress force oscillation. *Bioinspiration & Biomimetics*, *14*(6), 066001. doi: 10.1088/1748-3190/ab34fe

Lumley, J. L. (1970). *Stochastic tools in turbulence. volume 12. applied mathematics and mechanics* (Tech. Rep.). Pennsylvania State University, Department of Aerospace Engineering.

McClure, J., Morton, C., & Yarusevych, S. (2015). Flow development and structural loading on dual step cylinders in laminar shedding regime. *Physics of Fluids*, *27*(6), 063602. doi: 10.1063/1.4921491

Morton, C., & Yarusevych, S. (2020). Vortex shedding from cylinders with two step discontinuities in diameter. *Journal of Fluid Mechanics*, *902*. doi: 10.1017/jfm.2020.593

Owen, J., Bearman, P., & Szewczyk, A. (2001). Passive control of viv with drag reduction. *Journal of Fluids and Structures*, *15*(3), 597-605. doi: https://doi.org/10.1006/jfls.2000.0358

Tian, C., Jiang, F., Pettersen, B., & Andersson, H. I. (2020). Vortex dislocation mechanisms in the near wake of a step cylinder. *Journal of Fluid Mechanics*, *891*, A24. doi: 10.1017/jfm.2020.110

Williamson, C. H. K. (1992). The natural and forced formation of spot-like 'vortex dislocations' in the transition of a wake. *Journal of Fluid Mechanics*, *243*(-1), 393–441. doi: 10.1017/s0022112092002763

Zdravkovich, M. (1981). Review and classification of various aerodynamic and hydrodynamic means for suppressing vortex shedding. *Journal of Wind Engineering and Industrial Aerodynamics*, *7*(2), 145–189. doi: 10.1016/0167-6105(81)90036-2

Zdravkovich, M. M. (1996). Different modes of vortex shedding: an overview. *Journal of Fluids and Structures*, *10*(5), 427 437. doi: 10.1006/jfls.1996.0029